



Ignition Under Strained Conditions: A Comparison Between Instationary Counterflow and Non-premixed Flamelet Solutions

Z. Sun¹ · C. Hasse¹ · A. Scholtissek¹ 

Received: 3 December 2019 / Accepted: 12 July 2020 / Published online: 30 July 2020
© The Author(s) 2020

Abstract

The transient evolution of counterflow diffusion flames can be described in physical space [i.e. by the model of Im et al. (Combust. Sci. Technol. 158:341–363, 2000)], and in composition space through flamelet equations. Both modeling approaches are employed to study the ignition of diluted hydrogen–air, methane–air and DME–air diffusion flames including detailed transport and chemistry modeling. Using the physical space solution as a reference, this work elucidates the capability of flamelet modeling to predict ignition characteristics in terms of ignition temperature and ignition delay time. Varying pressure and strain rate for the hydrogen–air configurations, the agreement between reference solution and flamelet results is shown to strongly depend on the ignition limits as characterized by Kreutz and Law (Combust. Flame 104:157–175, 1996). In limit 2 and at elevated temperatures, where the ignition kernel formation is governed by chemical reactions and less dependent on mass transport (high Damköhler numbers), the flamelet model yields accurate results. Close to the ignition limits 1 and 3 however, significant deviations can be observed. In these limits, the residence time of radicals during ignition kernel formation is strongly influenced by diffusive transport and Damköhler numbers are low. The analysis of the hydrocarbon flames shows that differences between the physical space model and the flamelet model are smaller. This is attributed to a smaller influence of differential diffusion on the ignition process for methane and DME as compared to hydrogen as fuel. This paper underlines that flamelet models can be used to describe ignition processes under strained conditions, but care should be taken if ignition takes place in certain parameter ranges, i.e. close to the ignition limits or at high strain rates.

Keywords Ignition · Strain · Counterflow · Flamelet

✉ A. Scholtissek
scholtissek@stfs.tu-darmstadt.de

¹ Institute for Simulation of reactive Thermo-Fluid Systems, TU Darmstadt, Otto-Berndt-Straße 2, 64287 Darmstadt, Germany

1 Introduction

Counterflow diffusion flames have been essential for the research on fundamental flame physics and for the development of combustion models for both, laminar and turbulent combustion. The canonical counterflow flame can be described by a one-dimensional equation set (flow and chemistry) through a similarity transformation. Models which yield the steady state solution of a counterflow flame have been presented by Giovangigli and Smooke (1987) and Kee et al. (1989), and are widely used today. These models allow the efficient computation of fully resolved flame structures up to their strain-induced extinction limit including detailed transport and chemical kinetic models. Later, Im et al. (2000) presented an extended counterflow model which further consistently incorporates transient effects. With this model, also time-varying strain effects and ignition events can be studied in the counterflow configuration. However, additional numerical challenges arise solving the high index differential-algebraic equation system of this model and overall its group of users remained limited so far. Supposedly, one of the reasons for this is that transient effects in diffusion flames can also be efficiently described with flamelet-based models in composition space.

While the physical space counterflow models already allow a one-dimensional representation of the flame structure, flamelet models further separate the numerical solution of flow and mixing field from the solution of chemistry (Peters 1988; Pitsch et al. 1998). Flamelet models therefore require some sort of gradient information of the conditioning variable, which is the mixture fraction Z in case of non-premixed combustion. In the classical flamelet equations for temperature T and species mass fractions Y_k by Peters (1984, 1988) (derived for $Le_i = 1$)

$$\rho \frac{\partial T}{\partial \tau} = \frac{\rho \chi}{2} \frac{\partial^2 T}{\partial Z^2} + \dot{\omega}_T, \quad (1)$$

$$\rho \frac{\partial Y_k}{\partial \tau} = \frac{\rho \chi}{2} \frac{\partial^2 Y_k}{\partial Z^2} + \dot{\omega}_k, \quad (2)$$

this gradient information is contained in the scalar dissipation rate (SDR) $\chi = 2D|\nabla Z|^2$. In the above equation set, τ is a time-like coordinate, ρ denotes the density, and $\dot{\omega}_T$ and $\dot{\omega}_k$ are the chemical source terms of temperature and species k , respectively. Since Peters' original publication, flamelet models have been expanded to describe increasingly complex flame physics, such as differential diffusion (Pitsch and Peters 1998; Dietzsch et al. 2018), multi-feed combustion (Hasse and Peters 2005; Ihme and See 2011; Doran et al. 2013), enthalpy effects (Mittal et al. 2012), radiation and enhanced description of pollutant formation (Ihme and Pitsch 2008; Messig et al. 2013), unsteady effects (Cuenot et al. 2000; Pitsch 2000; Ihme and See 2010), and curvature-induced effects (Kortschik et al. 2005; Scholtissek et al. 2016).

Both, the physical space counterflow model by Im et al. (2000) and the unsteady flamelet model allow the computation of the transient evolution of counterflow diffusion flames, but χ is a solution quantity for the former and an input parameter for the latter (which usually requires modeling). Considering the physical space model as a reference, it is the objective of this work to elucidate the capabilities of flamelet modeling for capturing ignition characteristics of diffusion flames. Therefore, both modeling approaches are compared with respect to the ignition of diluted hydrogen-air, methane-air and DME-air diffusion flames and special attention is paid to the treatment of the SDR for flamelet modeling. Within the scope

of this work, we assess the accuracy of *commonly used modeling approaches* for the SDR, which have shown good results for predicting stationary flame structures and which have also been adopted in unsteady flamelet calculations (Pitsch and Ihme 2005; Claramunt et al. 2006; Ihme and See 2010). For the hydrogen flames, the physical space reference configuration corresponds to two counterflowing jets of 60% H₂/N₂ versus heated air for which an ignition event can be recorded if the oxidizer temperature is raised above the *ignition temperature* T_{ign} (the fuel-side temperature is kept constant at $T = 300$ K). Furthermore, the *ignition delay time* t_{ign} is defined as the time span for the system to reach a maximum temperature increase. The same configuration and procedure is used in the analysis of the hydrocarbon flames, only the N₂-dilution is reduced in the fuel stream (80% CH₄/N₂ and 80% DME/N₂, respectively). Predictions of the different models for T_{ign} and t_{ign} are compared and analyzed varying pressure and strain rate.

This paper is structured as follows: in the next section, the transient counterflow model is briefly revisited. Thereafter, an unsteady flamelet model incorporating detailed transport and chemistry is presented. Subsequently, both modeling approaches are verified by demonstrating a close agreement with recently published results from the literature and are then utilized to study the ignition of diluted hydrogen-air diffusion flames in detail, varying pressure and strain conditions. Subsequently, the analogous analysis for methane- and DME-flames is performed. The paper closes with summary and conclusions.

2 Transient Counterflow Model (TCF)

The transient counterflow (TCF) model utilized here is equivalent to the model presented by Im et al. (2000). It is assumed that the relevant physical quantities are a function of time t and the axial coordinate x only. The equations for the density ρ , the axial velocity u , the scaled radial velocity $V = v/r$, temperature T and the species mass fractions Y_k read

$$\begin{aligned} \frac{\partial \rho}{\partial t} + \frac{\partial(\rho u)}{\partial x} + 2\rho V &= \frac{\rho}{p_{\text{tot}}} \frac{\partial p_h}{\partial t} - \frac{\rho}{T} \frac{\partial T}{\partial t} \\ &- \rho \bar{W} \sum_{k=1}^K \frac{1}{W_k} \frac{\partial Y_k}{\partial t} + \frac{\partial(\rho u)}{\partial x} + 2\rho V = 0, \end{aligned} \tag{3}$$

$$\rho \frac{\partial u}{\partial t} + \rho u \frac{\partial u}{\partial x} = - \frac{\partial p_h}{\partial x} + 2\mu \frac{\partial V}{\partial x} - \frac{4}{3} \frac{\partial(\mu V)}{\partial x} + \frac{4}{3} \frac{\partial}{\partial x} \left(\mu \frac{\partial u}{\partial x} \right), \tag{4}$$

$$\rho \frac{\partial V}{\partial t} + \rho u \frac{\partial V}{\partial x} = - \Lambda(t) - \rho V^2 + \frac{\partial}{\partial x} \left(\mu \frac{\partial V}{\partial x} \right), \tag{5}$$

$$\begin{aligned} \rho c_p \frac{\partial T}{\partial t} + \rho u c_p \frac{\partial T}{\partial x} &= \frac{\partial p_h}{\partial t} + u \frac{\partial p_h}{\partial x} \\ &- \rho \sum_{k=1}^{n_s} c_{p,k} Y_k V_k \frac{\partial T}{\partial x} + \frac{\partial}{\partial x} \left(\lambda \frac{\partial T}{\partial x} \right) - \sum_{k=1}^{n_s} \dot{\omega}_k h_k, \end{aligned} \tag{6}$$

$$\rho \frac{\partial Y_k}{\partial t} + \rho u \frac{\partial Y_k}{\partial x} = - \frac{\partial \rho Y_k V_k}{\partial x} + \dot{\omega}_k W_k, \quad (k = 1, \dots, n_s), \tag{7}$$

where the radial pressure eigenvalue is defined as

$$\Lambda(t) \equiv \frac{1}{r} \frac{\partial p_h}{\partial r}, \quad (8)$$

which has to be solved as part of the solution. Here, the total pressure is decomposed into ambient reference pressure and the hydrodynamic pressure, $p_{\text{tot}} = p + p_h$. In the above equation set $\dot{\omega}_k$ is the net production rate of species k , c_p is the specific heat capacity, λ is the thermal conductivity, h_k is the enthalpy of species k , and \bar{W} and W_k denote the molecular masses of the mixture and of the k th species, respectively. The diffusion velocity V_k is computed from a mixture-averaged diffusion model (Curtiss and Hirschfelder 1949) with a correction term to ensure mass conservation (Coffee and Heimerl 1981).

The boundary conditions for the flow are chosen such that they satisfy the strain rate definition by Seshadri and Williams (1978)

$$k = \frac{2(u_f \sqrt{\rho_f / \rho_{\text{ox}}} - u_{\text{ox}})}{L}, \quad (9)$$

and a momentum balance between the two opposed jets, $\rho_f u_f^2 = \rho_{\text{ox}} u_{\text{ox}}^2$. The subscripts f and ox denote conditions in the fuel and oxidizer stream, respectively. For temperature and species, Dirichlet boundary conditions are imposed.

3 Flamelet Model (FLT)

A recently published flamelet (FLT) model (Dietzsch et al. 2018) allowing for detailed transport and chemistry is utilized in this work. The model is formulated with respect to the conditioning variable mixture fraction which is defined by the source-term-free transport equation

$$\frac{\partial \rho Z}{\partial t} + \nabla \cdot (\rho \mathbf{u} Z) = \nabla \cdot (\rho D_Z \nabla Z), \quad (10)$$

where the diffusion coefficient is chosen such that the Lewis number of Z equals unity, $D_Z = \lambda / (\rho c_p)$. The flamelet equations for temperature and species mass fraction read (Dietzsch et al. 2018)

$$\begin{aligned} \rho c_p \frac{\partial T}{\partial \tau} &= \frac{\chi}{2D_Z} \frac{\partial}{\partial Z} \left(\lambda \frac{\partial T}{\partial Z} \right) \\ &\quad - \frac{\chi}{2D_Z} \frac{\partial \rho D_Z}{\partial Z} \frac{\partial T}{\partial Z} - \frac{\rho \chi}{2D_Z} \sum_{k=1}^{n_s} c_{p,k} Y_k \tilde{V}_k \frac{\partial T}{\partial Z} - \sum_{k=1}^{n_s} h_k \dot{\omega}_k, \end{aligned} \quad (11)$$

$$\begin{aligned} \rho \frac{\partial Y_k}{\partial \tau} &= - \frac{\chi}{2D_Z} \frac{\partial}{\partial Z} (\rho Y_k \tilde{V}_k) \\ &\quad - \frac{\chi}{2D_Z} \frac{\partial \rho D_Z}{\partial Z} \frac{\partial Y_k}{\partial Z} - \frac{1}{4} \left(\rho Y_k \tilde{V}_k + \rho D_Z \frac{\partial Y_k}{\partial Z} \right) \frac{\partial}{\partial Z} \left(\frac{\chi}{D_Z} \right) + \dot{\omega}_k, \end{aligned} \quad (12)$$

where \tilde{V}_k represents a diffusion velocity in Z -space defined by

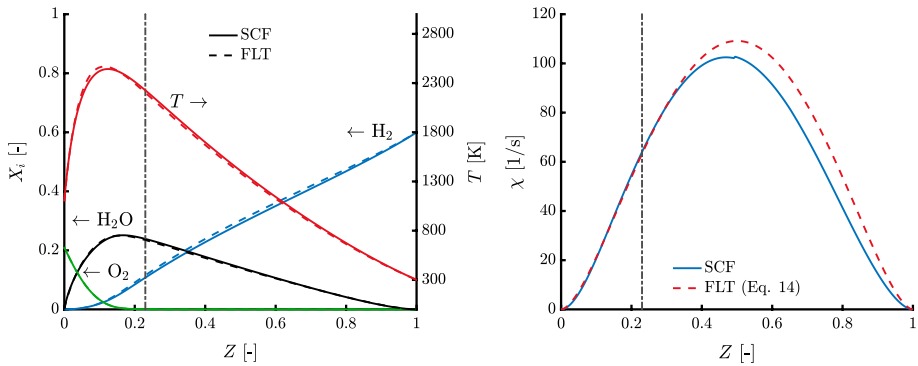


Fig. 1 Steady solution for a stationary counterflow diffusion flame (SCF, solid) together with the corresponding flamelet result (FLT, dashed line). The pressure is $p = 1$ atm, the fuel is 60% H_2/N_2 at $T_f = 300$ K and the oxidizer is air at $T_{ox} = 1100$ K. For both models, diffusion is modeled by the mixture-averaged method (Curtiss and Hirschfelder 1949) utilizing a correction velocity for mass conservation (Coffee and Heimerl 1981). Left: temperature and species profiles. Right: scalar dissipation rate profiles. For the flamelet model, χ is modeled by Eq. 14 and χ_{st} is matched to the SCF solution at stoichiometry ($Z_{st} = 0.23$)

$$Y_k \mathbf{V}_k = Y_k \tilde{V}_k \nabla Z. \tag{13}$$

This approach allows the usage of arbitrary diffusion models in mixture fraction space (i.e. Soret effect) (Dietzsch et al. 2018). Here, the transport model is chosen to match the TCF model discussed in the previous section, i.e. both approaches incorporate differential diffusion as described by the mixture-averaged formulation (Curtiss and Hirschfelder 1949; Coffee and Heimerl 1981). Note that the generalized flamelet equations given above can be reduced to the classical flamelet equations, Eqs. 1 and 2, by introducing a unity Lewis number diffusion model.

The scalar dissipation rate χ , which appears as a flamelet parameter in Eqs. 11 and 12, is either extracted from a TCF solution or defined by an analytical profile (Pitsch et al. 1998)

$$\chi(Z) = \chi_{st} \exp\left(2\left([\operatorname{erfc}^{-1}(2Z_{st})]^2 - [\operatorname{erfc}^{-1}(2Z)]^2\right)\right), \tag{14}$$

where the SDR at stoichiometric conditions¹ χ_{st} is chosen to match the physical space reference solution. Figure 1 shows the stationary solution for a 60% H_2/N_2 -air counterflow diffusion flame together with the corresponding flamelet result. For the latter, χ is modeled according to Eq. 14 and differences are observed on the rich side of the flame (c.f. Fig. 1, right). However, the close agreement of temperature and species profiles (c.f. Fig. 1, left) illustrates that Eq. 14 is an appropriate model for the scalar dissipation rate.

¹ Z_{st} is defined as the value of Z_{Bilger} at stoichiometry (Bilger 1976). Even though Z is defined based on Eq. (10) and formally decoupled from the species composition, Z_{st} is still regarded as a satisfactory estimate for the location of stoichiometry in Z -space (Pitsch and Peters 1998).

4 Results and Discussion

First, the models described above are briefly verified with results from the literature. Thereafter, they are used to study the ignition process (ignition temperature, ignition delay time) in a counterflow of diluted hydrogen (60% H_2/N_2) versus heated air. For this purpose, three different modeling approaches are introduced:

1. TCF, the transient counterflow model
2. FLT-1, the flamelet model initialized with the inert mixing solution and the χ -profile extracted from TCF (after initialization χ remains fixed)
3. FLT-2, the flamelet model initialized with an inert mixing solution obtained in composition space and with χ modeled by Eq. 14 (χ_{st} matches initial condition of TCF)

After its verification, the TCF model is treated as the reference solution in the remainder of the paper. The initial condition for this model is the inert mixing of fuel and oxidizer. It is obtained by switching off the chemical source terms in Eqs. 6 and 7 and integrating the problem until the stationary state is reached. As previously stated, for the TCF model flow and chemistry are dynamically linked and solved together during the ignition process. On the other hand, the models FLT-1 and FLT-2 only consider the chemistry solution with external flow information inherently prescribed through the SDR. For three reasons the SDR is fixed versus time for both flamelet modeling approaches: Firstly, as will be shown below, the SDR remains almost constant during the formation and growth of the ignition kernel until the ignition event. Secondly, Fig. 1 demonstrates that conditions for hydrogen-air counterflow flames can be accurately captured in mixture fraction space by modeling the SDR (c.f. Eq. 14) even if small deviations are observed in the χ -profile. Thirdly, transient SDR data is usually unavailable for the application of flamelet models. It should be noted that the ignition process can be modeled more accurately with a flamelet (FLT) model when scaling the scalar dissipation rate (SDR) at the ignition kernel position in Z -space. The exact location of the ignition kernel strongly depends on the fuel-oxidizer mixture, the temperature and the strain rate. Therefore, the ignition kernel position is not known prior to a flamelet calculation and would, in fact, require a TCF calculation. However, the latter would already provide the numerical solution for the ignition process making the flamelet calculation redundant.

Along these lines, FLT-1 can be understood as the best case scenario for a direct application of the flamelet model, for which the initial condition and the initial χ -profile is equivalent to the TCF model. The main difference between TCF and FLT-1 is that TCF is directly coupled to the solution of the flow while FLT-1 uses a static SDR profile. For the model FLT-2 on the other hand, χ is modeled by Eq. 14 with χ_{st} prescribed from the TCF solution and the inert mixing solution is obtained solely in mixture fraction space. This would be the procedure when employing the flamelet model for creating a chemistry table to be coupled to a CFD solver. In comparison, FLT-1 implicitly contains equivalent flow conditions during the ignition kernel formation as the TCF model while FLT-2 only uses Z_{st} and χ_{st} as scaling parameters. In both cases, FLT-1 and FLT-2, the fixation of the χ -profile introduces a static environment for the formation of the ignition kernel. Although this is not fully compliant with the TCF model, for which χ is a solution quantity and changes with time, it is the guiding question of this work how well the two flamelet modeling approaches recover ignition characteristics varying pressure and strain rate.

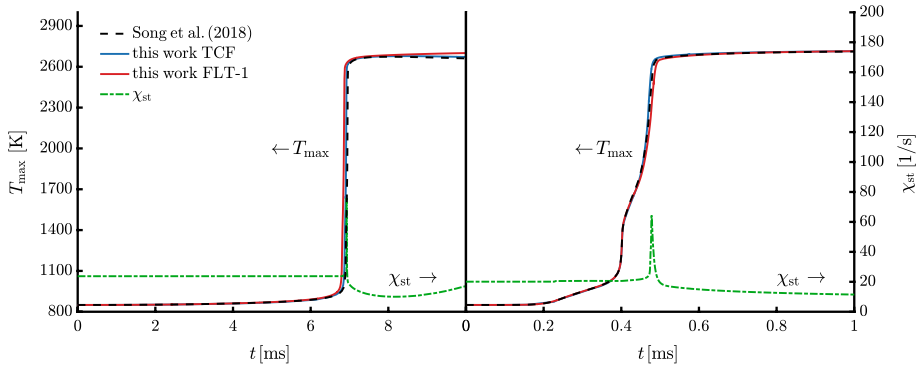


Fig. 2 Temporal evolution of temperature for pure MeOH (left) and a 50% MeOH/50% DME blend (right) during ignition. In both cases the oxidizer is air, $T_f = T_{ox} = 850$ K and the ambient pressure is $p = 40$ atm. The figure shows results obtained by Song et al. (2018) in comparison to results obtained with the models TCF and FLT-1

4.1 Verification

The implementation of the transient counterflow model (TCF) is verified with recent results by Song et al. (2018) who utilized the model to compute the ignition delay time of methanol (MeOH)/dimethyl ether (DME) blends. Two cases from their publication are considered: (a) pure MeOH, (b) 50% MeOH/50% DME, where the oxidizer is air. Both fuel and oxidizer temperature are set to 850 K and the ambient pressure is 40 atm. For the computations a reduced Aramco 1.3 mechanism (Song et al. 2018) is used, which was kindly provided by the authors. Figure 2 shows a comparison between the results by Song et al. (2018) and the results obtained with the models TCF and FLT-1 for the evolution of the maximum temperature during ignition. It is found that the ignition delay time and the evolution of the maximum temperature for MeOH and the MeOH/DME blend are accurately recovered by both the TCF and the FLT-1 model. Deviations between the FLT-1 model and the data from Ref. Song et al. (2018) is below 1%, and the TCF model shows smaller deviations. In Fig. 2, the temporal evolution of the stoichiometric scalar dissipation rate is shown, which confirms that the SDR remains nearly unchanged during formation and growth of the ignition kernel as stated earlier.

4.2 Ignition Temperatures of Diluted Hydrogen–Air Diffusion Flames

Kreutz and Law (1996) have shown that the ignition temperature T_{ign} varies according to three characteristic limits, which are similar to the explosion limits of homogeneous premixed fresh gases. These limits correspond to characteristic Z-shaped curves in the $p - T_{ign}$ diagram which are shown in Fig. 3 for the 60% H_2/N_2 -air flames studied here. The following considerations are based on the original work by Kreutz and Law (1996): In *limit 2*, the ignition kernel formation is mostly governed by chemical reactions. The production and destruction rates of relevant radicals (H, O, OH) are at least an order of magnitude larger than contributions of diffusive and convective transport to their overall budgets. This limit can therefore be well approximated by equating the most important chain-branching to the most important chain-terminating reaction governing

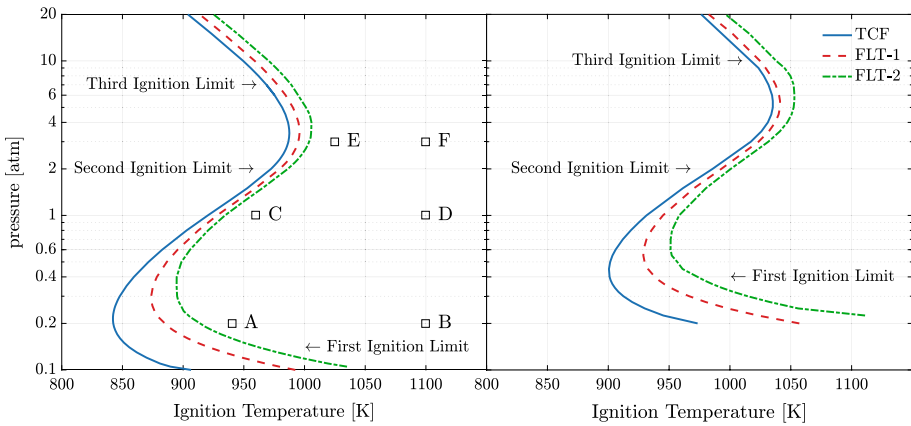


Fig. 3 Z-shaped curves (Kreutz and Law 1996) which mark the ignition limits for 60% H_2/N_2 -air diffusion flames in the $p - T_{\text{ign}}$ diagram for two different density weighted strain rates (left: $\tilde{k} = 200 \text{ s}^{-1}$, right: $\tilde{k} = 1000 \text{ s}^{-1}$). The plots show a comparison of the results obtained with the models TCF (solid), FLT-1 (dashed) and FLT-2 (dash-dotted). Besides the three characteristic ignition limits, six conditions (A–F) are marked in the left figure which are analyzed in more detail in terms of the ignition delay further below

the evolution of the radical pool of the ignition kernel. When the pressure is lowered, in *limit 1* chain-terminating reactions become more inhibited relative to chain-branching reactions such that mixtures can ignite at lower temperatures. However, diffusive transport, which influences the residence time of radicals in the ignition kernel, gains importance relative to the chemical reactions such that ignition temperatures rise again below a certain pressure level (lower turning point). In the high pressure limit 3, new chemical pathways become important (particularly for the species HO_2 and H_2O_2), which turn chain-terminating reaction pathways into chain-propagation pathways. Hence, ignition temperatures decrease again above a certain pressure level (upper turning point).

While the pressure is varied, the density weighted strain rate \tilde{k} , rather than the strain rate k , is held fixed (Kreutz and Law 1996)

$$\tilde{k} = \frac{\rho_{\text{ox}}}{\rho_{\text{ox}}^0} k. \quad (15)$$

In the above expression, the factor $\rho_{\text{ox}}/\rho_{\text{ox}}^0$ is the oxidizer density over the reference density at atmospheric pressure and $T = T_{\text{ign}}$, respectively. Fixing this strain rate ensures that the pre-ignition flow field remains invariant when varying oxidizer temperatures and pressure (Kreutz and Law 1996). In this work, the ignition temperature is defined as the lowest oxidizer temperature that leads to an ignition event within 1000 s (physical time). The ignition temperature is determined through a bisection search. The procedure starts from two independent simulations with different oxidizer temperatures at the boundary. It requires the mixture with the higher oxidizer temperature to be ignitable while the mixture with the lower oxidizer temperature is non-ignitable (within the time limit). The algorithm then proceeds carrying out further (independent) calculations while reducing the temperature difference and stops when this difference is smaller than 0.1 K. This algorithm has been compared to the approach by Kreutz and Law (1996) and it was found that both yield consistent results.

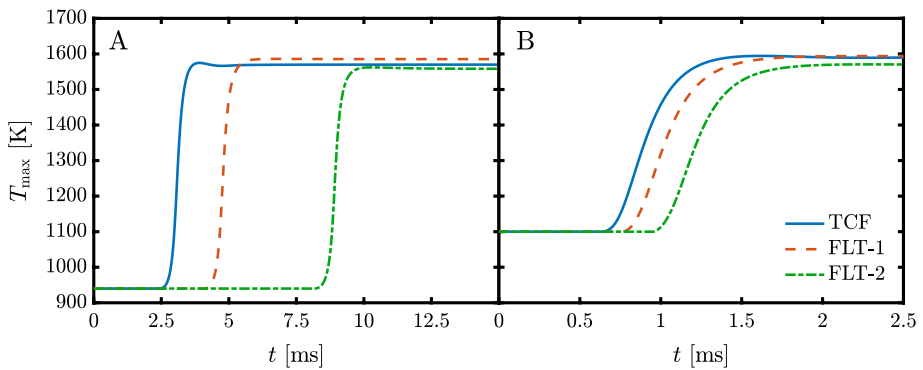


Fig. 4 Temporal evolution of T_{\max} versus time during ignition for $p = 0.2 \text{ atm}$ and $\bar{k} = 200 \text{ s}^{-1}$. Left: conditions close to the ignition limit 1 ($T_{\text{ox}} = 940 \text{ K}$). Right: for elevated oxidizer temperature ($T_{\text{ox}} = 1100 \text{ K}$)

In Fig. 3, the predictions for the ignition temperature of the three models TCF, FLT-1 and FLT-2 are shown. For all hydrogen flame calculations, the chemical mechanism by Varga et al. (2015) is used. Notably, the flamelet models can qualitatively recover the ignition characteristics such as the “Z-shape”. Nevertheless, in Fig. 3 large quantitative deviations between TCF and the flamelet models are observed close to the turning points and especially throughout limit 1 (low pressure limit). In the latter case, deviations from the TCF ignition temperature were larger than 50 K (FLT-1) and 100 K (FLT-2). Although χ only varies slightly before ignition takes place (c.f. Fig. 2), the flamelet models cannot capture the ignition temperatures obtained with the TCF model. Nonetheless, FLT-1 shows better agreement with TCF than FLT-2 which is due to the well-approximated initial conditions and SDR profile. Throughout the limits 2 and 3, FLT-1 shows reasonable agreement with TCF, where deviations for T_{ign} are below 10 K. FLT-2 exhibits larger deviations than FLT-1, which can clearly be attributed to the SDR-model and the not fully compliant initial conditions before ignition. Qualitatively, these trends are preserved when considering higher strain rates (c.f. Fig. 3, right) for which the Z-shaped curve becomes shifted in direction of the upper right corner of the diagram. This is important, since limit 1, where flamelet modeling shows the least accurate predictions of ignition temperatures, is shifted towards atmospheric pressures which are relevant conditions for certain technical combustion systems. In summary, these results illustrate that flamelet models overestimate ignition temperatures at low pressures and at high strain rates for the diluted hydrogen-air diffusion flames studied in this work.

4.3 Ignition Delay Times of Diluted Hydrogen–Air Diffusion Flames

Next, six different cases (A–F) are analyzed with respect to the ignition delay time. These cases are marked in terms of pressure and air-side temperature in Fig. 3 (left). The cases A, C, E are chosen close to the ignition limits while elevated oxidizer temperatures ($T_{\text{ox}} = 1100 \text{ K}$) are specified for the cases B, D, F.

Figure 4 shows the temporal evolution of the maximum temperature during ignition for the cases A and B. The plot shows the results of the three models TCF, FLT-1 and FLT-2, respectively. The boundary conditions for case A is chosen close to the ignition limit 1, while case B is further away from the limit ($T_{\text{ox}} = 1100 \text{ K}$). For case A, it is

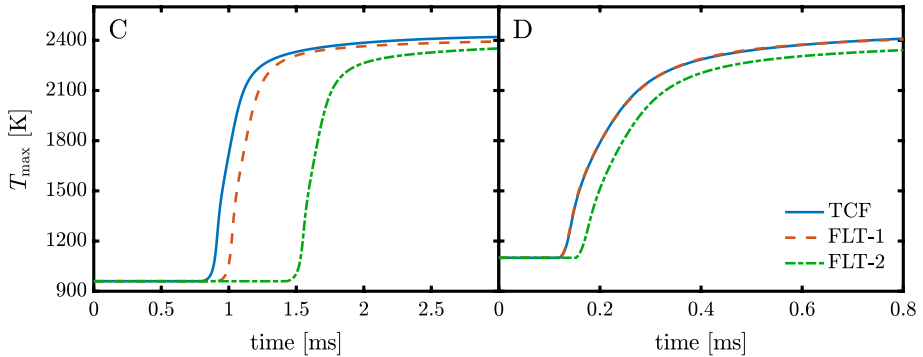


Fig. 5 Temporal evolution of T_{\max} versus time during ignition for $p = 1.0$ atm and $\tilde{k} = 200$ s $^{-1}$. Left: conditions close to the ignition limit 2 ($T_{\text{ox}} = 960$ K). Right: for elevated oxidizer temperature ($T_{\text{ox}} = 1100$ K)

found that both flamelet models largely overpredict the ignition delay time compared to the reference solution (FLT-1: 53%, FLT-2: 187%). For case B, the agreement between reference solution and flamelet results is improved, but still significant deviations are found (FLT-1: 15%, FLT-2: 38%). As Kreutz and Law (1996) state, the ignition in limit 1 is governed by both chemical reactions and diffusive transport. It can therefore be anticipated that chemical reactions, which are promoted much stronger by temperature than diffusive processes, govern the ignition process at elevated temperatures. Thus, modeling errors introduced by inaccurate modeling of diffusive time scales (i.e. the fixation of χ for FLT-1 and FLT-2) is less influential for the ignition process. Note that the final steady state conditions obtained after the ignition event differ among the three models. This is expected since the SDR is allowed to change for the TCF model, while different SDR profiles (specified as initial conditions) are held fixed for the flamelet modeling approaches. Due to the fact that the conditions prior to an ignition event are relevant for the evolution of the ignition kernel, differing steady state solutions do not alter the conclusions drawn here.

For cases C and D, the temporal evolution of the maximum temperature versus time is shown in Fig. 5. Case C is chosen close to the ignition limit 2 and an elevated oxidizer temperature is specified for case D (c.f. Fig. 3, left). Overall, the deviations between the flamelet models and the reference TCF model are smaller than for the corresponding cases A and B. The FLT-1 model overestimates the ignition delay time by 12% for case C and accurately recovers t_{ign} for case D (0.1% deviation). For FLT-2, still significant deviations from the reference are observed in both cases (case C: 70%, case D: 22%). Again, an increase of the oxidizer temperature T_{ox} promotes chemical reactions and eventually leads to a better prediction of the ignition delay by the flamelet models.

For the cases E and F shown in Fig. 6, the pressure is set to $p = 3$ atm. Thereby, case E is located at the turning point between ignition limit 2 and 3 along the Z-shaped curve (c.f. Fig. 3, left). Similar as before, an increased oxidizer temperature is specified for the second case, F. The inspection of the ignition delay times for case E shows that the flamelet models perform poorly close to the ignition limit (deviation of FLT-1: 68% and FLT-2: 282%). On the other hand, for case F, FLT-1 shows a close agreement (deviation: 0.5%) but FLT-2 still exhibits significant deviation from the reference (deviation: 79%).

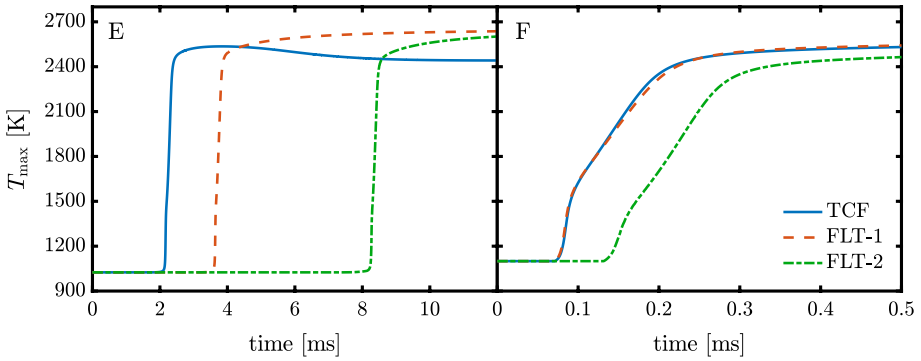


Fig. 6 Temporal evolution of T_{\max} versus time during ignition for $p = 3.0 \text{ atm}$ and $\bar{k} = 200 \text{ s}^{-1}$. Left: conditions close to the ignition limit 3 ($T_{\text{ox}} = 1025 \text{ K}$). Right: for elevated oxidizer temperature ($T_{\text{ox}} = 1100 \text{ K}$)

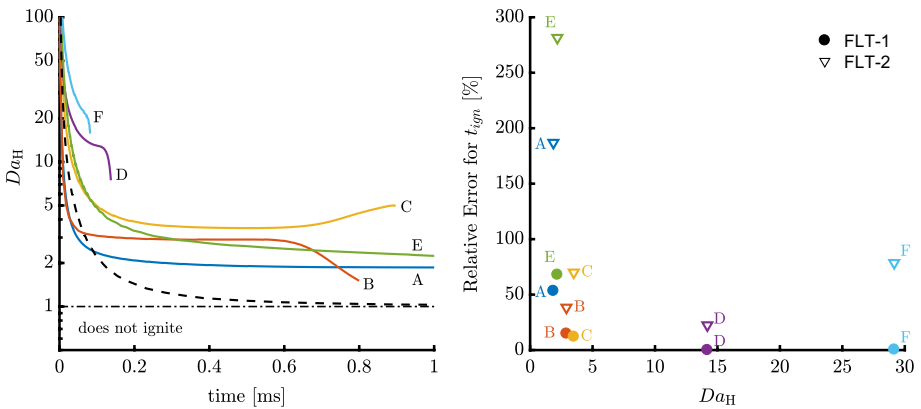


Fig. 7 Left: evolution of the Damköhler number Da_H at the peak position of the H-radical for cases A-F up to the ignition event (maximum temperature increase). If Da_H falls below unity, ignition is likely to fail (Mason et al. 2002). Right: deviation of the ignition delay time between FLT models and TCF reference result as a function of the Damköhler number

4.4 Damköhler Numbers for Diluted Hydrogen–Air Diffusion Flames

Mason et al. (2002) introduced a criterion for transient ignition by tracking the time evolution of an instantaneous species Damköhler number. It is defined as

$$Da_i = \left| \frac{\dot{\omega}_i}{\rho u (\partial Y_i / \partial x) + \partial (\rho Y_i V_i) / \partial x} \right|_{\text{kernel}}, \tag{16}$$

where the subscript “kernel” denotes the kernel location identified with the maximum H-radical concentration. The definition is based on a species balance equation and the H-radical equation is chosen as the reference due to its relevance for the ignition process of hydrogen–air diffusion flames.

Flamelet models are derived for the limit of large Damköhler numbers, or, in other words, when chemical time scales are significantly smaller than flow time scales.

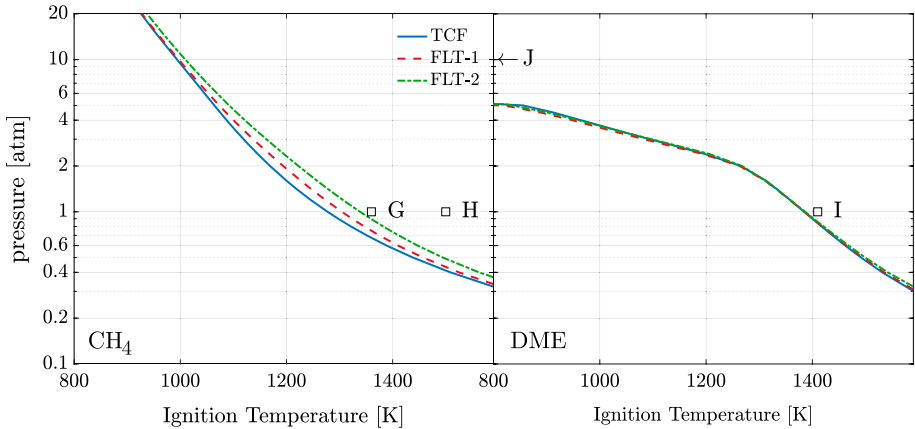


Fig. 8 Ignition limits for 80% CH₄/N₂-air (left) and 80% DME/N₂-air diffusion flames in the $p - T_{\text{ign}}$ diagram. Strain rates are chosen as $\bar{k} = 200 \text{ s}^{-1}$ (CH₄-flames) and $\bar{k} = 500 \text{ s}^{-1}$ (DME-flames). Results obtained with the model TCF (solid) are compared to corresponding flamelet solutions from FLT-1 (dashed) and FLT-2 (dash-dotted). Further, four conditions (G–J) are marked in the figures which are analyzed in terms of the ignition delay further below

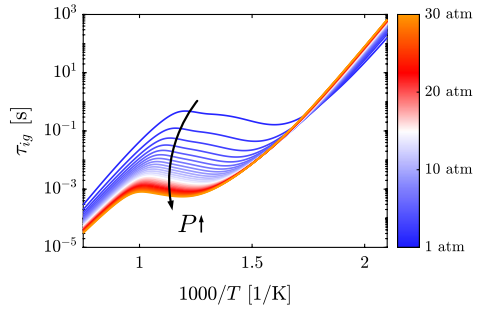
Furthermore, according to Mason et al. (2002), ignition will not take place if Da_{H} falls below unity. Thus, the definition given in Eq. 16 is supposedly also a suitable criterion for assessing the performance of flamelet modeling for ignition under strained conditions. The evolution of Da_{H} up to the ignition event is shown in Fig. 7 for the cases A–F. As expected, the Damköhler number increases when increasing the oxidizer temperature (compare cases A–B, C–D, E–F). Furthermore, the Damköhler number for the cases close to the ignition limit (A, C, E) is largest for case C which corresponds to ignition limit 2. This is consistent with the line of argument of Kreutz and Law (1996) and also with the good predictions of the flamelet models for ignition temperatures and ignition delay times. On the other hand, predictions of the flamelet models significantly deviate from TCF for lower Damköhler numbers (c.f. cases A, B, E). This trend is confirmed by considering the relative error of the ignition delay times obtained with FLT-1 and FLT-2 as a function of Da_{H} (c.f. Fig. 7, right).

4.5 Ignition Temperatures of Diluted Hydrocarbon Diffusion Flames

The ignition characteristics of the hydrocarbon flames are analyzed analogously as before: first, the ignition temperatures are determined for different pressure levels, and second, the ignition delay times are investigated for selected cases holding the temperatures of fuel and oxidizer stream fixed. In all calculations, the GRI3.0 mechanism (Smith et al. 1999) is utilized for methane flames and the mechanism by Zhao et al. (2008) for DME flames.

Opposed to hydrogen flames, the hydrocarbon flames considered here do not exhibit a “Z-shape” in the $p - T_{\text{ign}}$ diagram as observed from Fig. 8. Instead, a distinct trend is observed for both, methane (Fig. 8, left) and DME flames (Fig. 8, right), showing that an increase in pressure allows ignition with significantly lower oxidizer temperatures (and vice versa). Nevertheless, the response to strain rate is similar: increasing the strain rate shifts the ignition limits to larger T_{ign} (not shown).

Fig. 9 Ignition delay time for a homogeneous, stoichiometric mixture of 80% DME/N₂ and air as a function of temperature (i.e. zero strain solution)



The predictions of FLT-1 and FLT-2 for the ignition temperatures qualitatively recover these trends. Quantitatively, there are deviations between the flamelet results and the TCF reference solution in case of the methane flames, but very close agreement is observed for the DME flames. For methane, FLT-1 exhibits deviations for T_{ign} of 27 K and FLT-2 of 62 K at atmospheric pressures with respect to the TCF reference solution. These deviations decline towards higher and lower pressures, respectively. For DME, the deviations between flamelet and reference solutions are below 2 K. Notably, for DME the ignition temperature declines rapidly towards higher pressures allowing mixtures to be ignited at comparably low temperatures. This is due to the low-temperature chemistry of this fuel. However, at high pressure and low temperature the ignition process can take very long such that it becomes difficult to determine the ignition temperature. Essentially, it is not always clear whether a mixture cannot ignite below the determined ignition temperature or if the simulation runtime was too short to record the ignition event. This aspect is further illustrated in Fig. 9 which shows the ignition delay times for a homogeneous stoichiometric mixture of 80% DME/N₂ and air. It is observed, that the ignition delay time can theoretically become of the order of 10³ s at low temperatures and large pressures. Note that Fig. 9 solely underlines the time scale of the ignition process and is not quantitatively comparable to the ignition of the (strained) diffusion flame configuration.

4.6 Ignition Delay Times of Diluted Hydrocarbon Diffusion Flames

In the following, four cases (G–J) are examined with respect to the ignition delay times. These cases are marked in Fig. 8 and refer to two methane flame configurations and two DME flame configurations.

Figure 10 shows the temporal evolution of the maximum flame temperature for the diluted methane-air flames (cases G and H). For case G, the oxidizer temperature is chosen close to the ignition limit ($T_{\text{ox}} = 1360$ K) while case H exhibits an elevated oxidizer temperature ($T_{\text{ox}} = 1500$ K). Similar as for the diluted hydrogen-air flames, the increase in oxidizer temperature promotes the chemical reactivity of the mixture such that the ignition delay time is reduced and the influence of diffusion on the ignition process declines. Since diffusion modeling (i.e. representation of the SDR) marks the main difference between TCF and FLT, predictions of these models for τ_{ign} agree better for larger temperatures. Though, both flamelet modeling approaches lead to an overprediction of the ignition delay time, and, as expected, it is found that FLT-1 reproduces τ_{ign} more accurately (deviation for case G: 11%, case H: 1%) than FLT-2 (deviation for case G: 54%, case H: 7%).

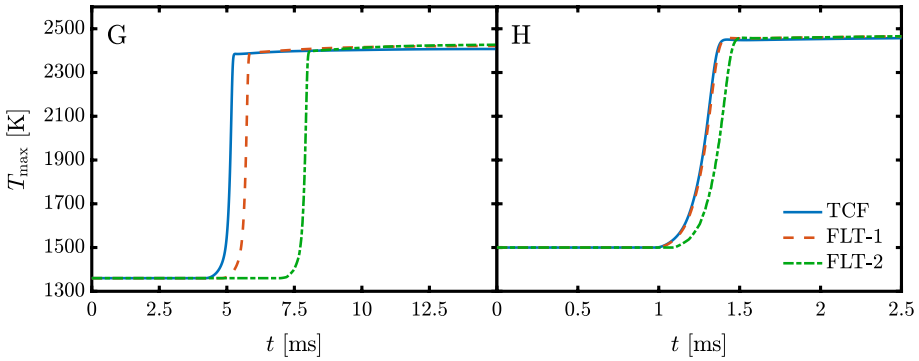


Fig. 10 Temporal evolution of T_{\max} versus time during ignition of 80% CH_4/N_2 -air diffusion flames for $p = 1.0$ atm and $\bar{k} = 200 \text{ s}^{-1}$. Left: conditions close to the ignition limit ($T_{\text{ox}} = 1360$ K). Right: for elevated oxidizer temperature ($T_{\text{ox}} = 1500$ K)

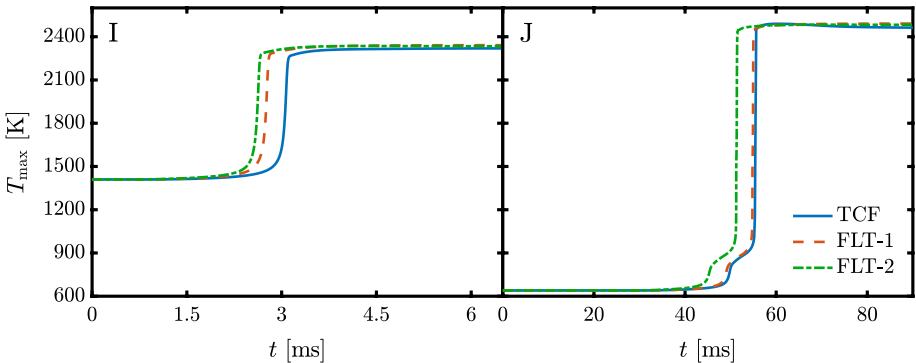


Fig. 11 Temporal evolution of T_{\max} versus time during ignition of 80% DME/N_2 -air diffusion flames at $\bar{k} = 500 \text{ s}^{-1}$. Left: conditions at atmospheric pressure, $p = 1.0$ atm and $T_{\text{ox}} = 1410$ K. Right: conditions at elevated pressure, $p = 10.0$ atm and oxidizer temperature $T_{\text{ox}} = 640$ K

For the diluted DME-air flames, predictions of ignition temperatures from FLT agree well with the TCF reference solution, but there are differences for the predictions of the ignition delay time. Case I (c.f. Fig. 8) represents conditions close to the ignition limit at atmospheric pressure and is thereby comparable to the cases C (hydrogen flames) and G (methane flames). The evolution of the maximum flame temperature for this case is shown in Fig. 11 (left). Overall, the agreement between TCF reference solution and FLT models is comparable to the methane flame in case G. Though, one notable difference is that both flamelet models underpredict the ignition delay time compared to the TCF model (deviations for FLT-1: -10% and FLT-2: -14%).

Case J is specifically chosen at high pressure ($p = 10.0$ atm) and comparably low oxidizer temperature $T_{\text{ox}} = 640$ K. Due to the low-temperature chemistry of DME, ignition is still possible in this parameter range and as shown in Fig. 11 (right), two-stage ignition behavior can be observed for this case. It is found that both flamelet models recover the two-stage ignition characteristics with FLT-1 showing a close agreement (-1% deviation) and FLT-2 only a moderate underprediction (-7% deviation).

5 Summary and Conclusions

Ignition processes of diluted hydrogen-air, methane-air and DME-air diffusion flames are studied employing a transient counterflow (TCF) model formulated in the physical space, and a transient flamelet (FLT) model formulated in mixture fraction space. The TCF model is utilized to compute the ignition process in opposed streams of fuel versus heated air. An ignition event under strained conditions can be recorded if the air-side temperature is raised above the so-called ignition temperature. Furthermore, starting from a stationary inert mixing solution allows to compute an ignition delay time. Both characteristic quantities can also be computed in mixture fraction space and are used to assess the capability of the flamelet model to capture ignition, treating the TCF model as a reference. For this assessment, two common flamelet modeling approaches are defined: the FLT-1 model is initialized with the same inert mixing solution and scalar dissipation rate profile as the TCF model. For the FLT-2 model, the inert mixing solution is computed directly in mixture fraction space and the scalar dissipation rate is modeled.

For the comparison of the models TCF, FLT-1 and FLT-2 ignition temperatures are determined varying pressure and strain rate. As shown by Kreutz and Law (1996), three ignition limits can be identified for the hydrogen flames in the $p - T_{\text{ign}}$ diagram (Z-shaped curve). While the flamelet models qualitatively recover all three limits, quantitatively large differences are observed in comparison to the TCF reference in certain parameter ranges. Flamelet modeling particularly shows large deviations for ignition limit 1 (low pressure limit) where Damköhler numbers are low and diffusive processes influence the residence times of radicals during formation of the ignition kernel. The ignition limit 2 is governed by chemical reactions, Damköhler numbers are increased, and diffusive transport is less influential. For this limit, both flamelet models reasonably capture ignition temperatures. In the transition region between ignition limit 2 and 3 (elevated pressures), ignition kernel formation can again be influenced by transport effects. For that parameter range, FLT-1 still shows acceptable agreement with the reference TCF model while FLT-2 shows significant deviations.

Thereafter, three ignition processes close to the ignition limits 1-3 and three ignition processes at the analogous pressure levels, but with higher oxidizer temperatures, are examined in terms of the ignition delay time. Similar trends as for the ignition temperatures are observed: the flamelet models reasonably recover ignition delay times in limit 2 and at elevated temperatures, but show significant deviations close to the ignition limits 1 and 3.

The analysis of the hydrocarbon flames shows a distinct trend in the $p - T_{\text{ign}}$ diagram: increasing the pressure decreases the ignition temperature and vice versa. Furthermore, the predictions of the ignition temperatures by flamelet modeling is more accurate for the hydrocarbon flames compared to the hydrogen flames. Particularly for DME, the predictions for the ignition temperature are recovered within 2 K by both, FLT-1 and FLT-2. The investigation of corresponding ignition delay times revealed similar trends as for the hydrogen-flames: when sufficiently removed from the ignition limit, flamelet predictions for τ_{ign} become more accurate. Additionally, it is shown for DME-flames that two-stage ignition behavior is also captured in flamelet-space.

These results suggest that, in the general case, the physical space TCF model is required for an accurate prediction of ignition events under strained conditions. This modeling approach is essential if transport processes influence the formation and growth of the ignition kernels. On the other hand, it is shown that flamelet modeling works well in certain parameter ranges, particularly if chemistry governs the ignition kernel formation (ignition

limit 2 for hydrogen-flames or high temperatures in general). It is further found that modeling the scalar dissipation rate using a common analytical profile leads to non-negligible modeling errors for ignition processes even at higher Damköhler numbers. It remains to be shown whether flamelet modeling can overcome some of these limitations when applied in the context of tabulated chemistry approaches.

Acknowledgements Open Access funding provided by Projekt DEAL. Funding is kindly acknowledged from the Deutsche Forschungsgemeinschaft (DFG, German Research Foundation) Project numbers 325144795 and 310695286.

Compliance with Ethical Standards

Conflict of interest The authors declare that they have no conflict of interest.

Open Access This article is licensed under a Creative Commons Attribution 4.0 International License, which permits use, sharing, adaptation, distribution and reproduction in any medium or format, as long as you give appropriate credit to the original author(s) and the source, provide a link to the Creative Commons licence, and indicate if changes were made. The images or other third party material in this article are included in the article's Creative Commons licence, unless indicated otherwise in a credit line to the material. If material is not included in the article's Creative Commons licence and your intended use is not permitted by statutory regulation or exceeds the permitted use, you will need to obtain permission directly from the copyright holder. To view a copy of this licence, visit <http://creativecommons.org/licenses/by/4.0/>.

References

- Bilger, R.W.: The structure of diffusion flames. *Combust. Sci. Technol.* **13**, 155–170 (1976)
- Claramunt, K., Cònsul, R., Carbonell, D., Segarra, C.P.: Analysis of the laminar flamelet concept for non-premixed laminar flames. *Combust. Flame* **145**, 845–862 (2006)
- Coffee, T.P., Heimerl, J.M.: Transport algorithms for premixed, laminar steady-state flames. *Combust. Flame* **43**, 273–289 (1981)
- Cuenot, B., Egolfopoulos, F., Poinso, T.: An unsteady laminar flamelet model for non-premixed combustion. *Combust. Theor. Model.* **4**, 77–97 (2000)
- Curtiss, C.F., Hirschfelder, J.O.: Transport properties of multicomponent gas mixtures. *J. Chem. Phys.* **17**, 550–555 (1949)
- Dietzsch, F., Scholtissek, A., Hunger, F., Hasse, C.: The impact of thermal diffusion on the structure of non-premixed flames. *Combust. Flame* **194**, 352–362 (2018)
- Doran, E.M., Pitsch, H., Cook, D.J.: A priori testing of a two-dimensional unsteady flamelet model for three-feed combustion systems. *Proc. Combust. Inst.* **34**, 1317–1324 (2013)
- Giovangigli, V., Smooke, M.: Calculation of extinction limits for premixed laminar flames in a stagnation point flow. *J. Comput. Phys.* **68**, 327–345 (1987)
- Hasse, C., Peters, N.: A two mixture fraction flamelet model applied to split injections in a DI diesel engine. *Proc. Combust. Inst.* **30**, 2755–2762 (2005)
- Ihme, M., Pitsch, H.: Modeling of radiation and nitric oxide formation in turbulent nonpremixed flames using a flamelet/progress variable formulation. *Phys. Fluids* **20**, 055110 (2008)
- Ihme, M., See, Y.C.: Prediction of autoignition in a lifted methane/air flame using an unsteady flamelet/progress variable model. *Combust. Flame* **157**, 1850–1862 (2010)
- Ihme, M., See, Y.C.: LES flamelet modeling of a three-stream MILD combustor: Analysis of flame sensitivity to scalar inflow conditions. *Proc. Combust. Inst.* **33**, 1309–1317 (2011)
- Im, H.G., Raja, L.L., Kee, R.J., Petzold, L.R.: A numerical study of transient ignition in a counterflow non-premixed methane-air flame using adaptive time integration. *Combust. Sci. Technol.* **158**, 341–363 (2000)
- Kee, R.J., Miller, J.A., Evans, G.H., Dixon-Lewis, G.: A computational model of the structure and extinction of strained, opposed flow, premixed methane-air flames. *Symp. (Int.) Combust.* **22**, 1479–1494 (1989)

- Kortschik, C., Honnet, S., Peters, N.: Influence of curvature on the onset of autoignition in a corrugated counterflow mixing field. *Combust. Flame* **142**, 140–152 (2005)
- Kreutz, T., Law, C.: Ignition in nonpremixed counterflowing hydrogen versus heated air: computational study with detailed chemistry. *Combust. Flame* **104**, 157–175 (1996)
- Mason, S.D., Chen, J., Im, H.G.: Effects of unsteady scalar dissipation rate on ignition of non-premixed hydrogen/air mixtures in counterflow. *Proc. Combust. Inst.* **29**, 1629–1636 (2002)
- Messig, D., Hunger, F., Keller, J., Hasse, C.: Evaluation of radiation modeling approaches for non-premixed flamelets considering a laminar methane air flame. *Combust. Flame* **160**, 251–264 (2013)
- Mittal, V., Cook, D.J., Pitsch, H.: An extended multi-regime flamelet model for IC engines. *Combust. Flame* **159**, 2767–2776 (2012)
- Peters, N.: Laminar diffusion flamelet models in non-premixed turbulent combustion. *Prog. Energy Combust. Sci.* **10**, 319–339 (1984)
- Peters, N.: Laminar flamelet concepts in turbulent combustion. *Symp. (Int.) Combust.* **21**, 1231–1250 (1988)
- Pitsch, H., Ihme, M.: An unsteady/flamelet progress variable method for LES of nonpremixed turbulent combustion. In: 43rd AIAA Aerospace Sciences Meeting and Exhibit (2005)
- Pitsch, H.: Unsteady flamelet modeling of differential diffusion in turbulent jet diffusion flames. *Combust. Flame* **123**, 358–374 (2000)
- Pitsch, H., Peters, N.: A consistent flamelet formulation for non-premixed combustion considering differential diffusion effects. *Combust. Flame* **114**, 26–40 (1998)
- Pitsch, H., Chen, M., Peters, N.: Unsteady flamelet modeling of turbulent hydrogen-air diffusion flames. *Symp. (Int.) Combust.* **27**, 1057–1064 (1998)
- Scholtissek, A., Pitz, R., Hasse, C.: Flamelet budget and regime analysis for non-premixed tubular flames. *Proc. Combust. Inst.* **36**, 1349–1356 (2016)
- Seshadri, K., Williams, F.: Laminar flow between parallel plates with injection of a reactant at high Reynolds number. *Int. J. Heat Mass Transf.* **21**, 251–253 (1978)
- Smith, G.P., Golden, D.M., Frenklach, M., Moriarty, N.W., Eiteneer, B., Goldenberg, M., Bowman, C.T., Hanson, R.K., Song, S., Gardiner Jr., W.C., Lissianski, V.V., Qin, Z.: Gri-mech 3.0 (1999)
- Song, W., Tingas, E.-A., Im, H.G.: A computational analysis of methanol autoignition enhancement by dimethyl ether addition in a counterflow mixing layer. *Combust. Flame* **195**, 84–98 (2018)
- Varga, T., Nagy, T., Olm, C., Zsély, I., Pálvölgyi, R., Valkó, É., Vincze, G., Cserhádi, M., Curran, H., Turányi, T.: Optimization of a hydrogen combustion mechanism using both direct and indirect measurements. *Proc. Combust. Inst.* **35**, 589–596 (2015)
- Zhao, Z., Chaos, M., Kazakov, A., Dryer, F.L.: Thermal decomposition reaction and a comprehensive kinetic model of dimethyl ether. *Int. J. Chem. Kinet.* **40**, 1–18 (2008)